This is the accepted manuscript made available via CHORUS. The article has been published as:

Diameter dependence of thermoelectric power of semiconducting carbon nanotubes

Nguyen T. Hung, Ahmad R. T. Nugraha, Eddwi H. Hasdeo, Mildred S. Dresselhaus, and Riichiro Saito

Phys. Rev. B **92**, 165426 — Published 21 October 2015

DOI: 10.1103/PhysRevB.92.165426

Diameter dependence of thermoelectric power of semiconducting carbon nanotubes

Nguyen T. Hung[1],* Ahmad R. T. Nugraha[1],† Eddwi H. Hasdeo[1], Mildred S. Dresselhaus[2,3], and Riichiro Saito[1]
[1]*Department of Physics, Tohoku University, Sendai 980-8578, Japan*
[2]*Department of Electrical Engineering, Massachusetts Institute of Technology, Cambridge, MA 02139-4307, USA*
[3]*Department of Physics, Massachusetts Institute of Technology, Cambridge, MA 02139-4307, USA*
(Dated: October 5, 2015)

We calculate the thermoelectric power (or thermopower) of many semiconducting single wall carbon nanotubes (s-SWNTs) within a diameter range 0.5–1.5 nm by using the Boltzmann transport formalism combined with an extended tight-binding model. We find that the thermopower of s-SWNTs increases as the tube diameter decreases. For some s-SWNTs with diameters less than 0.6 nm, the thermopower can reach a value larger than $2000\,\mu$V/K at room temperature, which is about 6 to 10 times larger than that found in commonly used thermoelectric materials. The large thermopower values may be attributed to the one-dimensionality of the nanotubes and to the presence of large band gaps of the small-diameter s-SWNTs. We derive an analytical formula to reproduce the numerical calculation of the thermopower and we find that the thermopower of a given s-SWNT is directly related with its band gap. The formula also explains the shape of the thermopower as a function of tube diameter, which looks similar to the shape of the so-called Kataura plot of the band gap dependence on tube diameter.

PACS numbers: 79.10.-n,72.20.Pa,65.80.-g

I. INTRODUCTION

In recent years, there has been significant interest in research on thermoelectric phenomena due to the increase in the demand for alternative energy sources. Especially, since thermoelectric phenomena could transform heat currents into electric power, thermoelectric power generators can perhaps be used to convert waste heat into electric energy for use in environmentally friendly applications [1–3]. It is thus necessary to find a good thermoelectric material with a high thermoelectic energy conversion efficiency, characterized by the so-called thermoelectric figure of merit, $ZT = S^2\sigma\kappa^{-1}T$, where S is the Seebeck coefficient, also known as the thermoelectric power (thermopower), σ is the electrical conductivity, κ is the thermal conductivity, and T is the absolute temperature of the material. Over the past six decades it has been challenging to obtain ZT values exceeding 2, because the parameters of ZT are generally interdependent [2, 3]. A theoretical study in 1993 predicted that the ZT value of low-dimensional structures could be significantly enhanced, thanks to the quantum confinement effect to create sharp features in the density-of-states (DOS) [4]. This prediction was confirmed experimentally in 1996 using PbTe/$Pb_{1-x}Eu_xTe$, which exhibited a ZT value up to about five times greater than that of the corresponding bulk value [5]. It is thus intriguing to evaluate other low-dimensional structures that might have excellent thermoelectric performance, either theoretically or experimentally.

As a one-dimensional material, single wall carbon nanotubes (SWNTs) were considered promising for thermoelectric materials due to their novel electronic properties which depend on their geometrical structure [6–8]. However, it has been difficult to obtain an ensemble of individual SWNTs with a specific (n, m) structure to reveal the precise knowledge of the dependence of the thermoelectric power of individual SWNTs on band gap and diameter. Most thermoelectric measurements were performed on bundled SWNT samples whose geometrical and electronic structures are complex [6–9], and thus the potential thermoelectric properties might have been lost because of interactions between different tubes [6]. The ZT values reported for bundled SWNTs have remained in the range of 10^{-3} to 10^{-4} [9, 10], in contrast to the commercial thermoelectric materials with $ZT \approx 1$ [11, 12]. Such bundled SWNT samples consist of a collection of SWNTs with different diameters, metallicities, and chiralities, parameters to which the electronic structure is very sensitive [13]. The small ZT value of the bundled SWNTs were mainly attributed to their low thermopower and high thermal conductivity, which might be a result of the mixture of different SWNTs and impurity in low concentration in the samples.

In this work, we will focus on evaluating the thermopower theoretically for many SWNTs, especially in the case of semiconducting SWNTs (s-SWNTs), and thus to maximize the SWNT thermopower and to suggest a new route for obtaining a larger ZT for SWNTs. By calculating the thermopower of all individual s-SWNTs within a diameter range $0.5 \le d_t \le 1.5$ nm, we will show that, for tube diameters less than 0.6 nm under low doping, the thermopower of s-SWNTs can be as large as $2000\,\mu$V/K at room temperature, which is large enough compared to the thermopower of bundled SWNTs, which is about $100 - 200\,\mu$V/K [6, 8, 14]. From this result, we believe that there is still much room available to improve the ZT of SWNT samples. For a more practical pur-

* nguyen@flex.phys.tohoku.ac.jp
† nugraha@flex.phys.tohoku.ac.jp

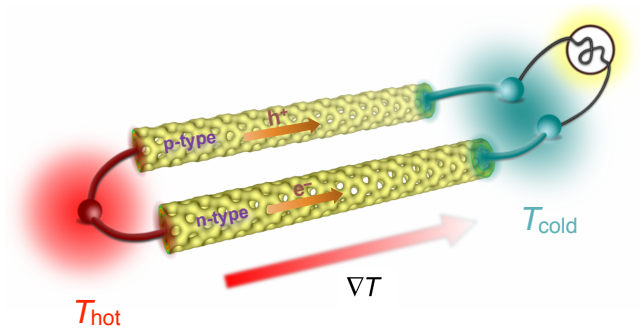

FIG. 1. (Color online) Schematic model of a thermoelectric device using two identical s-SWNTs, one with p-type and the other with n-type doping. The temperature gradient between the two edges of each nanotube generates an electric current.

pose, we also give an analytical formula to reproduce our numerical calculation of the s-SWNT thermopower, which forms a map of the s-SWNT thermopower. The calculated thermopower map could be useful for obtaining information on the s-SWNT chirality with a desired thermopower value and thus it offers promise for using specially prepared s-SWNT samples to guide the direction of future research on the thermoelectricity.

This paper is organized as follows. In Sec. II, we give the theoretical methods employed in this study to calculate the thermopower. In Sec. III, we discuss the thermopower obtained from the numerical calculation and compare it with the analytical formula. We then summarize the results and give the future perspective in Sec. IV. We also provide some appendices for a detailed derivation of the thermopower analytical formula.

II. MODEL AND METHODS

To utilize the s-SWNTs as a main material in future thermoelectric devices, we consider a model shown in Fig. 1, in which two identical s-SWNTs, one with p-type and the other with n-type doping, are connected in parallel. Each s-SWNT should maintain its electronic charge distribution in the nonequilibrium state, for example, by a temperature gradient along the tube axis. By having their temperature gradient ∇T from an edge of each s-SWNT to its other edge, charge carriers (electrons or holes) will flow with velocity v from the hot edge with temperature $T_{\rm hot}$ to the cold edge with temperature $T_{\rm cold}$. The carrier distribution f_0, which depends on the electronic energy ε and chemical potential μ, is modified as a function of ε, following the Boltzmann transport formalism. Within such a process, an electric voltage ∇V can be generated. It is also known from earlier studies that the electron-phonon interaction is the main factor determining the electrical conductivity of SWNTs [15–17], in which the so-called twisting (TW) phonon mode with a long wavelength gives the dominant contribution to the electron-phonon interaction. In particular, Jiang *et al.* showed that the relaxation time from the electron scattering with the TW phonon mode is independent of the electron energy [17]. Therefore, here we make the assumption that the thermopower from the Boltzmann transport equation can be obtained by applying the relaxation time approximation (RTA) and we may even treat the relaxation time as a constant. Under the RTA, the thermopower or Seebeck coefficient S is expressed by

$$S = -\frac{\nabla V}{\nabla T} = \frac{1}{qT}\frac{\int v(\varepsilon)\tau(\varepsilon)v(\varepsilon)\frac{\partial f_0(\varepsilon)}{\partial \varepsilon}[\varepsilon-\mu]g(\varepsilon)d\varepsilon}{\int v(\varepsilon)\tau(\varepsilon)v(\varepsilon)\frac{\partial f_0(\varepsilon)}{\partial \varepsilon}g(\varepsilon)d\varepsilon}, \quad (1)$$

where $q = \pm e$ is the unit carrier charge, $T = (T_{\rm hot} + T_{\rm cold})/2$ is the average absolute temperature, $v(\varepsilon)$ is the carrier velocity, $g(\varepsilon)$ is the electronic (DOS), and $\tau(\varepsilon)$ is the carrier relaxation time.

We employ both numerical and analytical methods to obtain S from Eq. (1). In the full numerical approach, we can use the BoltzTraP code [18], which is a widely-used package to calculate some thermoelectric properties, such as the thermopower and electrical conductivity. A necessary input for the BoltzTraP code is the electronic energy dispersion $\varepsilon(k)$ for all bands (multiband structure). The BoltzTraP code also adopts a constant τ, whose plausibility in the case of s-SWNTs has been justified above. While the BoltzTraP code is actually sufficient for obtaining the thermopower from Eq. (1), we cannot discuss the physics of the thermopower of s-SWNTs without having an explicit formula for the thermopower that depends on some physical parameters, such as the SWNT band gap and geometrical structure. Therefore, we also solve Eq. (1) analytically by considering the valence band and the conduction band closest to the Fermi level, known as the two-band model [19, 20]. The derivation of the analytical formula is explained in detail in Appendices A-D.

As the input for the BoltzTraP code, we calculate the energy dispersion $\varepsilon(k)$ within the extended-tight binding (ETB) model developed in our group [21]. The ETB model takes into account long-range interactions, SWNT curvature corrections, and geometrical structure optimizations, which are sufficient to reproduce the experimentally observed energy band gaps of the SWNTs [21–23]. The SWNT structure in our notation is denoted by a set of integers (n, m) which is a shorthand for the chiral vector $\mathbf{C}_h = n\mathbf{a}_1 + m\mathbf{a}_2$, where $\mathbf{a}_1$ and $\mathbf{a}_2$ are the unit vectors of an unrolled graphene sheet [13]. The chiral vector $\mathbf{C}_h$ defines the circumferential direction of the tube, giving the diameter $d_{\rm t}$. Another vector perpendicular to $\mathbf{C}_h$ defines the tube axis, which is called the translational vector $\mathbf{T}$ [13]. The chiral and translational vectors thus represent the tube unit cell. In the BoltzTraP calculation, we use a $20\,{\rm nm} \times 20\,{\rm nm} \times |\mathbf{T}|$ supercell, where $|\mathbf{T}|$ (in

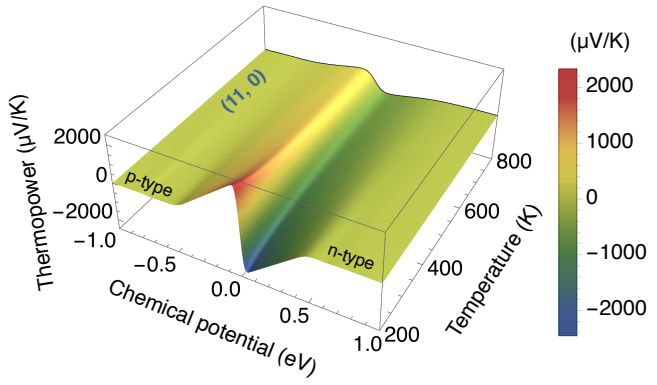

FIG. 2. (Color online) Thermopower as a function of chemical potential and temperature for an $(11,0)$ s-SWNT.

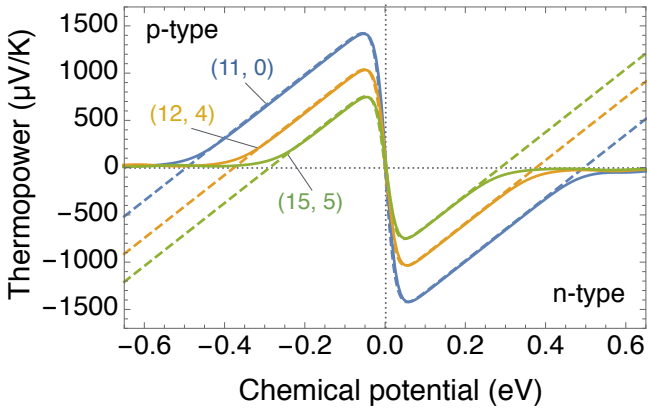

FIG. 3. (Color online) Thermopower as a function of chemical potential for $(11,0)$, $(12,4)$, and $(15,5)$ s-SWNTs at 300 K. Solid lines are obtained from the numerical calculation based on Eq. (1) while dashed lines are obtained from the analytical formula given in Eq. (2).

nm) is the length of the translational vector. A large supercell length in the x- and y-directions is chosen so as to guarantee the one-dimensionality of the SWNTs. Since the thermopower in the BoltzTraP code is expressed in terms of a tensor [18], the corresponding thermopower tensor component for a given s-SWNT is S_{zz}, which is the thermopower along the tube axis direction. Other tensor components are negligible.

III. RESULTS AND DISCUSSION

In Fig. 2, we show a first example of the thermopower calculation result for an $(11,0)$ s-SWNT. The thermopower (S_{zz}) is plotted versus chemical potential and temperature. We see that the thermopower is higher at the lower temperature because $S \propto 1/T$ in Eq. (1). The maximum thermopower obtained for the $(11,0)$ SWNT is about $1420\,\mu$V/K, which is already large for a purely individual s-SWNT compared to that for bundled SWNTs with S of around $100-200\,\mu$V/K [6, 8]. Next, we can also plot the thermopower at a specific temperature to see the chemical potential dependence of the thermopower. In Fig. 3, we show the thermopower versus chemical potential for three different s-SWNT chiralities: $(11,0)$, $(12,4)$, and $(15,5)$, at $T = 300\,$K. The solid lines in Fig. 3 represent the numerical results. For all chiralities, the optimum value of the thermopower, indicated by a maximum (minimum) along the negative (positive) axis of the chemical potential, arises due to the p-type (n-type) characteristics of the s-SWNTs, which is consistent with a recent experimental observation [8]. The dependence of the thermopower on the chemical potential implies that it is possible to tune the thermoelectric properties of s-SWNTs by applying a gate voltage, giving p-type and n-type control over the thermopower.

To better understand the numerical results of thermopower, we have derived an analytical formula for the thermopower within the two-band model [19, 20]. We denote this analytical formula of the thermopower as $S_{\rm CNT}$ (see Appendices A-D for the detailed derivation). The final form of $S_{\rm CNT}$ can be written as

$$S_{\rm CNT} = \frac{k_B}{e}\left(\frac{\mu}{k_BT} - \frac{E_g}{2k_BT} - \frac{3}{2} + \frac{E_g/k_BT+3}{e^{2\mu/k_BT}+1}\right), \quad (2)$$

where e is the elementary electric charge, k_B is the Boltzmann constant, and E_g is the SWNT band gap. The E_g values adopted in Eq. (2) are obtained from previous ETB results [21]. The dashed lines in Fig. 3 represent the fit of the numerical results of the thermopower using Eq. (2) for three different s-SWNT chiralities. The analytical formula [Eq. (2)] fits the numerical results near $\mu = 0$. In particular, the two optimum thermopower values (maximum and minimum for p-type and n-type doping, respectively) can be well-reproduced in that region, which implies that the energy bands near the Fermi level give the strongest contribution to the thermopower of s-SWNTs. The analytical results deviate from the numerical results at larger $|\mu|$ far from the optimum thermopower because the two-band model is no longer valid at a higher doping level. However, for the discussion in this paper, the two-band model is already sufficient to describe the thermopower of s-SWNTs since we will mainly focus on the optimum values of the thermopower.

For a more rigorous argument, we determine a condition to obtain an optimized chemical potential $\mu_{\rm opt}$ from Eq. (2), which satisfies $dS_{\rm CNT}(\mu_{\rm opt})/d\mu = 0$. We then obtain

$$\mu_{\rm opt} = \frac{k_BT}{2}\ln\left(\frac{E_g}{k_BT} + 2 \pm \sqrt{\left(\frac{E_g}{k_BT}+2\right)^2 - 1}\right), \quad (3)$$

where the $+$ and $-$ signs define the n-type and p-type contributions, respectively. From Eq. (3), we can say that the $\mu_{\rm opt}$ values will move more distant from $\mu = 0$ as E_g becomes larger than k_BT, as shown in Fig. 4(a). However, due to the presence of the logarithmic term, $\mu_{\rm opt}$ is very slowly changing as a function of E_g when E_g

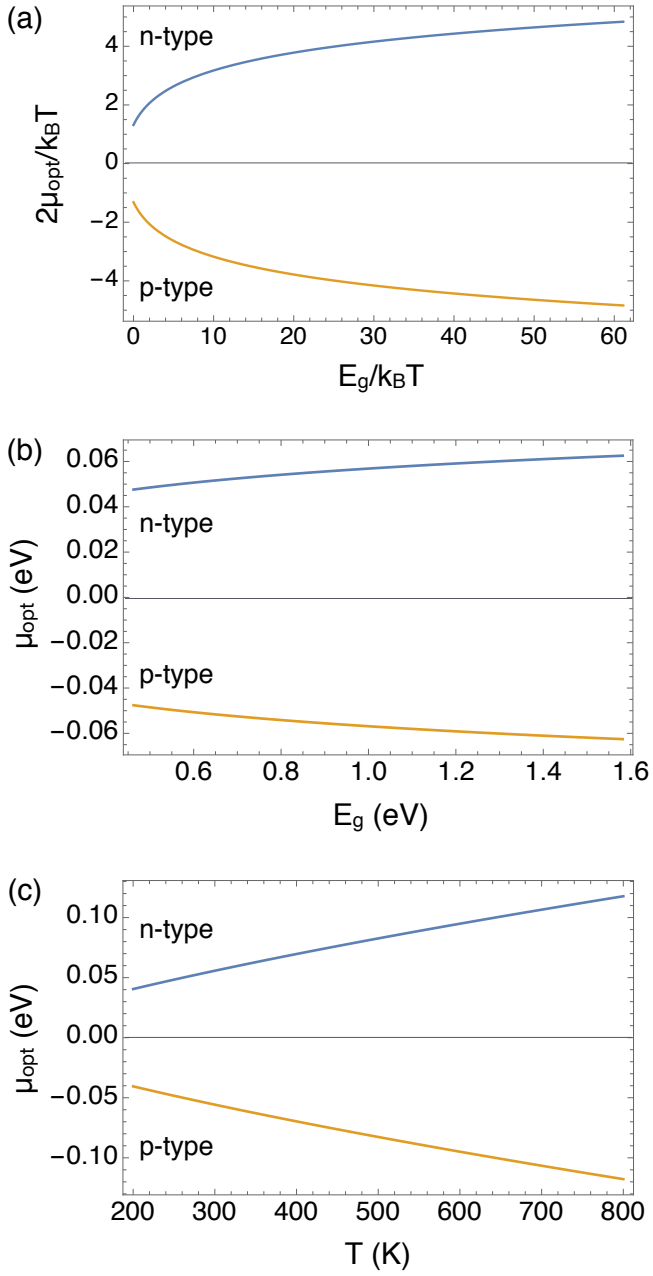

FIG. 4. (Color online) The optimized chemical potential $\mu_{\rm opt}$ plotted as a function of s-SWNT band gap. In panel (a), we scale the chemical potential and the band gap by $k_BT/2$ and k_BT, respectively, as described by Eq. (3). In the case of (b), we set a constant $T = 300$ K and vary E_g, while in (c) we set a constant $E_g = 0.913\,$eV, which is the band gap value of an $(11, 0)$ s-SWNT, and vary the temperature.

is much larger than k_BT. This behavior can be seen in Fig. 4(b), in which we show the E_g dependence of $\mu_{\rm opt}$. For the d_t range of 0.5–1.5 nm, the s-SWNTs have E_g values of about 1.58 eV down to 0.46 eV. In this case, E_g is about 17–61 times larger than k_BT for $T = 300$ K. With those E_g values, we then obtain $0.046 < |\mu_{\rm opt}| < 0.062\,$eV at a constant $T = 300\,$K [see Fig. 4(b)], which implies that the change in $\mu_{\rm opt}$ in this case is only about 16 meV although the change in E_g is as large as about 1.12 eV for the same d_t range. At room temperature, controlling the doping level or the chemical potential is thus useful to give us the optimum thermopower for the s-SWNTs under consideration. On the other hand, by decreasing T for a given E_g, we can also decrease $\mu_{\rm opt}$, as shown in Fig. 4(c), which reduces the doping level required to obtain the optimum thermopower. It should be noted that in Fig. 4(c) we intentionally set a constant $E_g = 0.913\,$eV for simplicity although the s-SWNT band gaps in the realistic case may decrease as a function of temperature by about 3% when we increase T from 200 K to 800 K [24].

Using both the numerical calculation by BoltzTraP and our analytical formula $S_{\rm CNT}$, it is now possible for us to plot the thermopower of s-SWNTs over a broad range of d_t by taking the optimum value of the thermopower. In the case of the analytical formula, we define the optimum thermopower $S^{\rm opt}_{\rm CNT}$ from Eqs. (2) and (3), as follows

$$S^{\rm opt}_{\rm CNT} = S_{\rm CNT}(\mu = \mu_{\rm opt}). \tag{4}$$

In Figs. 5(a-b), we show the optimum thermopower values of many s-SWNTs with $0.5 \le d_{\rm t} \le 1.5\,$nm compared with their corresponding band gaps as a function of diameter. In Fig. 5(a), we plot the optimum thermopower calculated from the BoltzTrap simulation (denoted by circles) and from $S^{\rm opt}_{\rm CNT}$ (denoted by plus symbols) on the same scale. We can see that the two methods show a good agreement. From Fig. 5(a), the thermopower of s-SWNTs is also found to increase as the tube diameter $d_{\rm t}$ decreases. For some s-SWNTs with $d_t < 0.6\,$nm, such as those with $2n + m = 13$, i.e. the $(5, 3)$ and $(6, 1)$ s-SWNTs, the thermopower can reach a value more than $2000\,\mu$V/K. These thermopower values are about 6–10 times larger than those found in common thermoelectric materials [12, 25–28].

The larger thermopower for smaller-diameter s-SWNTs can be explained by the relation of $S_{\rm CNT}$ with E_g as shown in Eq. (2) and by the fact that $E_g \propto 1/d_{\rm t}$ [29]. The one-dimensional character of the SWNT electronic DOS may also enhance the thermopower [4, 5]. Here, we should note that the thermopower of s-SWNTs as a function of diameter shows the nanotube family pattern, in which the different SWNTs with the same $2n + m$ can be connected and they make a clearly distinct branch for $\mathrm{mod}(2n+m, 3) = 1$ and $\mathrm{mod}(2n+m, 3) = 2$, known as the nanotube SI and SII family branches, respectively [29]. This behavior is very similar to that found in the band gap as a function of diameter shown in Fig. 5(b), which is often referred to as the Kataura plot [23, 29, 30]. This result also suggests that the measurement of the thermopower of a single chirality s-SWNT sample might be able to predict an exact band gap value of the s-SWNT. In fact, the band gap is directly connected to the thermopower as can be seen in the $S_{\rm CNT}$ formula [Eq. (2)].

Finally, we would like to briefly discuss the issues of maximizing the thermoelectric power factor, which is the

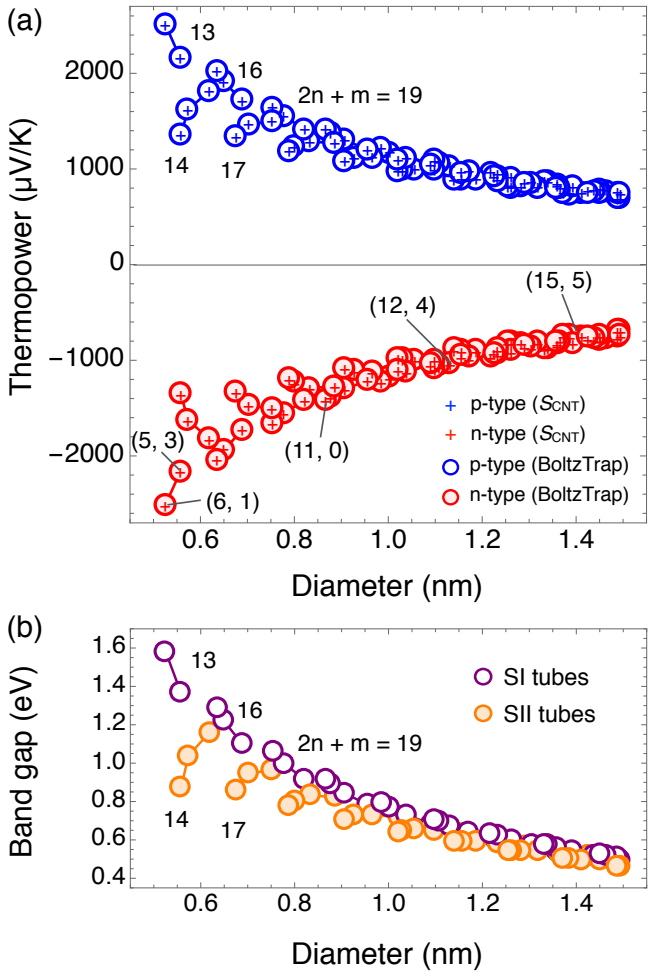

FIG. 5. (Color online) (a) Optimum thermopower $S^{\rm opt}_{\rm CNT}$ values for all s-SWNTs within the diameter range of 0.5–1.5 nm plotted as a function of SWNT diameter. The temperature is set constant at 300 K. Numerical results from BoltzTraP are denoted by circles, while analytical results from Eqs. (2)-(4) are denoted by plus symbols. (b) The Kataura plot showing the family pattern of the SWNT band gap as a function of diameter. Solid lines are a guide for the eyes, connecting SWNTs with the same family number $2n+m$. The SI and SII tubes correspond to the SWNTs having $\mathrm{mod}(2n+m, 3) = 1$ and 2, respectively.

numerator term in the ZT formula. There are two main issues to which we have to pay attention. First, we may argue that, for s-SWNTs as a thermoelectric material, it might still be impossible to obtain a large ZT or a usable device at a low doping level despite the fact that the optimum thermopower values are obtained near $\mu = 0$. The reason is that the electrical conductivity σ can be very small near $\mu = 0$. This fact is also reflected in the conductivity equation as a function of μ [see Appendix B, Eq. (B4)]. However, compared to the bulk materials, the one-dimensional materials such as s-SWNTs have smaller effective mass m^*, which may enhance the electrical conductivity due to the relation of $\sigma \propto (m^*)^{-1/2}$, as can also be seen in Eq. (B4). Second, we may worry that, as we go to smaller diameter s-SWNTs (in which the thermopower is optimized), the electrical conductivity will instead be too small to maximize the power factor. However, we note that there is also a chirality dependence which could enhance the electrical conductivity through the effective mass relation. As mentioned before, a smaller m^* will give a larger σ, and thus s-SWNTs which have both small diameters and small m^* might be useful as a thermoelectric material even at relatively low doping levels.

IV. SUMMARY

We have shown the theoretically predicted behavior of the thermopower of many s-SWNTs within a diameter range of 0.5–1.5 nm. We derive a simple formula to calculate the thermopower of s-SWNTs from their band gap, which enables us to predict the optimum thermopower values. The optimum thermopower value of an individual s-SWNT (p-type or n-type) can be larger than 2000 μV/K at room temperature for diameters less than 0.6 nm, such as the $(5, 3)$ and $(6, 1)$ s-SWNT. Our results highlight potential properties of small diameter s-SWNTs as a one-dimensional thermoelectric material with a giant thermopower. With the recent advances in the fabrication methods for specific small diameter s-SWNTs [14, 31, 32], we expect that the further potential development of s-SWNT thermoelectric devices could be realized in the near future.

ACKNOWLEDGMENTS

N.T.H. and A.R.T.N acknowledge the support from the Tohoku University Program for Leading Graduate Schools. R.S. acknowledges MEXT Grants Nos. 25107005 and 25286005. M.S.D acknowledges support from NSF grant DMR-1004147.

Appendix A: Thermopower of nondegenerate semiconductors

Here we derive a general formula for the thermopower of nondegenerate semiconductors as a starting point before deriving the analytical formula of $S_{\rm CNT}$ [Eq. (2)]. In the calculation of the thermopower, we assume that the single wall carbon nanotubes (s-SWNTs) are nondegenerate semiconductors. The thermopower or the Seebeck coefficient for a nondegenerate semiconductor can be calculated by solving the Boltzmann transport equation under the relaxation time approximation, which leads to the

following expression [20]:

$$S = \frac{1}{qT}\frac{\int \upsilon(\varepsilon)\tau(\varepsilon)\upsilon(\varepsilon)\frac{\partial f_0(\varepsilon)}{\partial \varepsilon}[\varepsilon-\mu]g(\varepsilon)d\varepsilon}{\int \upsilon(\varepsilon)\tau(\varepsilon)\upsilon(\varepsilon)\frac{\partial f_0(\varepsilon)}{\partial \varepsilon}g(\varepsilon)d\varepsilon}, \quad \text{(A1)}$$

where q, ε, T, and μ are the unit carrier charge, electronic band energy, temperature, and chemical potential, respectively. The variables $\upsilon(\varepsilon)$, $\tau(\varepsilon)$, $f_0(\varepsilon)$, and $g(\varepsilon)$ are the band carrier velocity, carrier relaxation (scattering) time, Fermi-Dirac distribution function, and the density of states (DOS) per unit volume, respectively, defined by

$$\upsilon^2(\varepsilon) = \frac{2\varepsilon}{m^* d}, \quad \text{(A2)}$$

$$\tau(\varepsilon) = \tau_0 \varepsilon^r, \quad \text{(A3)}$$

$$f_0(\varepsilon) = \frac{1}{1+e^{(\varepsilon-\mu)/k_B T}}, \quad \text{(A4)}$$

$$g(\varepsilon) = \frac{1}{L^{3-d}2^{d-1}\pi^{d/2}\Gamma\left(\frac{d}{2}\right)}\left(\frac{2m^*}{\hbar^2}\right)^{d/2}\varepsilon^{d/2-1}, \quad \text{(A5)}$$

where $d = 1, 2, 3$ denotes the dimension of the material, m^* is the effective mass of electrons or holes, r is a characteristic exponent, τ_0 is the relaxation time constant, and L is the confinement length for a particular material dimension. Substituting Eqs. (A2)-(A5) into Eq. (A1) yields

$$S = \frac{1}{qT}\left(\mu - \frac{\int \varepsilon^{d/2+r+1}\frac{\partial f_0(\varepsilon)}{\partial \varepsilon}d\varepsilon}{\int \varepsilon^{d/2+r}\frac{\partial f_0(\varepsilon)}{\partial \varepsilon}d\varepsilon}\right). \quad \text{(A6)}$$

To simplify Eq. (A6), we define the following variables: the reduced band energy $\xi = \varepsilon/(k_B T)$, the reduced chemical potential $\eta = \mu/(k_B T)$, and the Fermi-Dirac integral $F_j(\eta) = \int \xi^j f_0(\xi)d\xi$. Inserting these quantities into Eq. (A6) gives

$$S = -\frac{k_B}{q}\left(\eta - \frac{\frac{d}{2}+r+1}{\frac{d}{2}+r}\times\frac{F_{d/2+r}}{F_{d/2+r-1}}\right). \quad \text{(A7)}$$

Since $(\xi - \eta) > 3$ for nondegenerate semiconductors, we can use an approximation of $F_j(\eta) \approx e^{\eta}\Gamma(j+1)$, where $\Gamma(j)$ is the gamma function, to obtain

$$S = -\frac{k_B}{q}\left(\eta - \frac{\frac{d}{2}+r+1}{\frac{d}{2}+r}\times\frac{\Gamma(\frac{d}{2}+r+1)}{\Gamma(\frac{d}{2}+r)}\right). \quad \text{(A8)}$$

Using the recursion formula $\Gamma(j+1) = j\Gamma(j)$, the thermopower of nondegenerate semiconductors within the one-band model can be written as

$$S = -\frac{k_B}{q}\left(\eta - \frac{d}{2} - r - 1\right). \quad \text{(A9)}$$

This last equation is still insufficient to derive the thermopower of s-SWNTs since the s-SWNTs are considered as nondegenerate semiconductors with two energy bands. In this case, we also need an expression of electrical conductivity because the semiconductor within the two-band model includes a conduction band for electrons and a valence band for holes following the formula $S = (\sigma_n S_n + \sigma_p S_p)/(\sigma_n + \sigma_p)$ [19], where $S_{n,p}$ and $\sigma_{n,p}$ are, respectively, the thermopower and electrical conductivity for the n-type or p-type semiconductors. The expression specifying the electrical conductivity for a single energy band is derived in Appendix B.

Appendix B: Electrical conductivity for nondegenerate semiconductors

The electrical conductivity is expressed as [20]

$$\sigma = -q^2\int \upsilon(\varepsilon)\tau(\varepsilon)\upsilon(\varepsilon)\frac{\partial f_0(\varepsilon)}{\partial \varepsilon}g(\varepsilon)d\varepsilon. \quad \text{(B1)}$$

Substituting Eqs. (A2)-(A5) and the Fermi-Dirac integrals into Eq. (B1) yields

$$\sigma = \frac{2q^2\tau_0\left(\frac{d}{2}+r\right)}{m^* d}\frac{1}{L^{3-d}2^{d-1}\pi^{d/2}\Gamma(\frac{d}{2})}\left(\frac{2m^*}{\hbar^2}\right)^{d/2} \times (k_B T)^{d/2+r}F_{d/2+r-1}. \quad \text{(B2)}$$

By applying the approximation $F_j(\eta) \approx e^{\eta}\Gamma(j+1)$ for nondegenerate semiconductors, we can write the electrical conductivity,

$$\sigma = \frac{2q^2\tau_0\left(\frac{d}{2}+r\right)}{m^* d}\frac{1}{L^{3-d}2^{d-1}\pi^{d/2}\Gamma(\frac{d}{2})}\left(\frac{2m^*}{\hbar^2}\right)^{d/2} \times (k_B T)^{d/2+r}e^{\eta}\Gamma\left(\frac{d}{2}+r\right), \quad \text{(B3)}$$

which finally becomes

$$\sigma = \frac{2q^2\tau_0\left(\frac{d}{2}+r\right)(k_B T)^{d/2+r}\Gamma(\frac{d}{2}+r)}{d\ L^{3-d}2^{d/2-1}\pi^{d/2}\hbar^d\Gamma(\frac{d}{2})}(m^*)^{d/2-1}e^{\eta}. \quad \text{(B4)}$$

We will use Eq. (B4) for calculating the electrical conductivity to derive the thermopower of two-band semiconductors in the next section.

Appendix C: Thermopower of two-band semiconductors

The thermopower of two-band semiconductors is defined by [19]

$$S = \frac{\sigma_n S_n + \sigma_p S_p}{\sigma_n + \sigma_p}, \quad \text{(C1)}$$

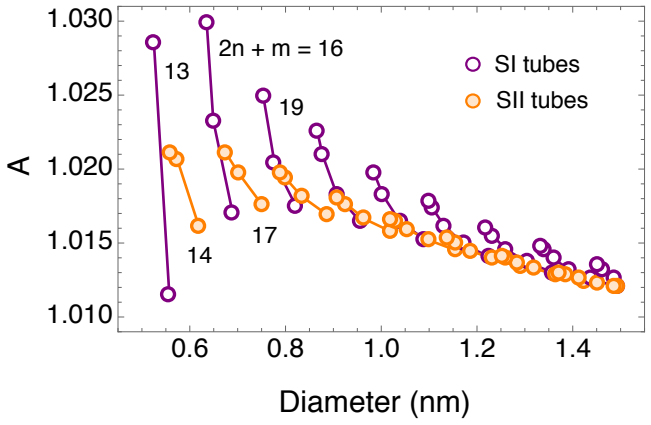

FIG. 6. $A = \left(m_n^*/m_p^*\right)^{-1/2}$ for s-SWNTs plotted as a function of the SWNT diameter. SI and SII tubes correspond to the SWNTs having $\mathrm{mod}(2n+m,3) = 1$ and 2, respectively. Solid lines connect SWNTs with the same $2n+m$ value.

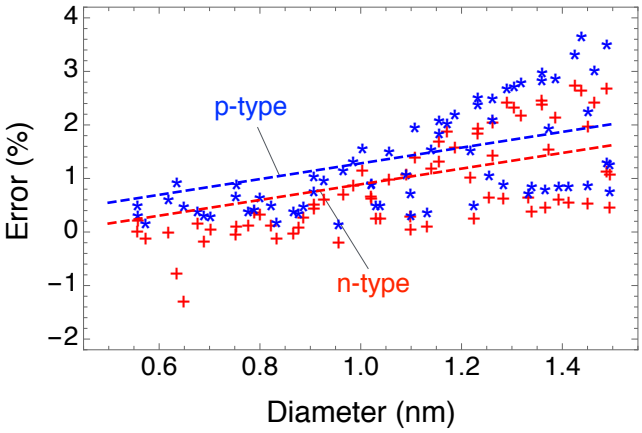

FIG. 7. (Color online) The percentage error, or the discrepancy between the analytical and the numerical results of the thermopower calculations for each s-SWNT, is plotted versus the SWNT diameter. The discrepancy increases linearly with increasing the SWNT diameter, as indicated by the fitted dashed lines.

where $\sigma_{n,p}$ and $S_{n,p}$ are expressed as

$$\sigma_{n,p} = \frac{2q^2\tau_0\left(\frac{d}{2}+r\right)(k_BT)^{d/2+r}\Gamma(\frac{d}{2}+r)}{d\,L^{3-d}2^{d/2-1}\pi^{d/2}\hbar^d\Gamma(\frac{d}{2})} \times (m_{n,p}^*)^{d/2-1}e^{\eta_{n,p}}, \tag{C2}$$

and

$$S_{n,p} = \mp\frac{k_B}{e}\left(\eta_{n,p} - \frac{d}{2} - r - 1\right), \tag{C3}$$

respectively. Substituting Eqs. (C2) and (C3) into Eq. (C1), and after doing some algebra, we can obtain

$$S = \frac{k_B}{e}\frac{\left(\eta_n - \frac{d}{2} - r - 1\right)\frac{\sigma_n}{\sigma_p} - \left(\eta_p - \frac{d}{2} - r - 1\right)}{\frac{\sigma_n}{\sigma_p} + 1}. \tag{C4}$$

where $\sigma_n/\sigma_p = \left(m_n^*/m_p^*\right)^{d/2-1} e^{\eta_n-\eta_p} = Ae^{\eta_n-\eta_p}$, with $A = \left(m_n^*/m_p^*\right)^{d/2-1}$. Here we have $\eta_n - \eta_p = 2\eta_\mu$ and $\eta_n + \eta_p = -\eta_g$, where $\eta_\mu = \mu/(k_BT)$ and $\eta_g = E_g/(k_BT)$. The thermopower of nondegenerate semiconductors within the two-band approximation can then be written in terms of η_μ, η_g, r, d, and A as

$$S = \frac{k_B}{e}\left(\eta_\mu - \frac{\eta_g}{2} - r - \frac{d}{2} - 1 + \frac{\eta_g + 2r + d + 2}{Ae^{2\eta_\mu}+1}\right). \tag{C5}$$

Appendix D: Thermopower of s-SWNTs

We now finally have all the information needed to derive S_{CNT}. Since s-SWNTs are one-dimensional, we have $d = 1$ and $A = \left(m_n^*/m_p^*\right)^{-1/2}$. The electron and hole effective masses $m_{n,p}^*$ in the s-SWNTs can be calculated using the effective mass formula $m^* = \hbar^2(d^2\varepsilon/dk^2)^{-1}$, where $\varepsilon(k)$ is the electronic energy dispersion within the extended tight binding (ETB) model [21]. We can obtain A as a function of diameter, as can be seen in Fig. 6, in which we show A within a diameter range of 0.5–1.5 nm. In this diameter range, we have $A \approx 1$. With such an approximation, and also assuming that the carrier relaxation time is constant [which gives $r = 0$ according to Eq. (A3)], the thermopower of s-SWNTs is then given by

$$S_{\mathrm{CNT}} = \frac{k_B}{e}\left(\eta_\mu - \frac{\eta_g}{2} - \frac{3}{2} + \frac{\eta_g+3}{e^{2\eta_\mu}+1}\right). \tag{D1}$$

The thermopower can be rewritten in terms of μ and E_g as

$$S_{\mathrm{CNT}} = \frac{k_B}{e}\left(\frac{\mu}{k_BT} - \frac{E_g}{2k_BT} - \frac{3}{2} + \frac{E_g/k_BT+3}{e^{2\mu/k_BT}+1}\right). \tag{D2}$$

where k_B is the Boltzmann constant and E_g is taken from the ETB calculation [21]. We see that Eq. (D2) is nothing but Eq. (2). In this derivation, the reason why we put $r = 0$ is that the electron relaxation time τ in s-SWNTs is determined mainly by the electron-phonon interaction with the TW phonon mode (see the main text, Sec. II), where the relaxation time is taken to be independent of the electron energy [17]. Therefore, we can write $\tau = \tau_0$ or equivalently $r = 0$.

Appendix E: Comparison between numerical and analytical methods

To verify the accuracy of the $S_{\mathrm{CNT}}^{\mathrm{opt}}$ in fitting the numerical results of the s-SWNT thermopower, we show

in Fig. 7 the difference of the thermopower obtained from the analytical and numerical calculations in terms of the error percentage. This error percentage variable is the difference in the thermopower calculated by using the $S_{\mathrm{CNT}}^{\mathrm{opt}}$ formula with respect to the numerical results for each s-SWNT diameter. We obtain the error values ranging from -2% to 4% for both p-type and n-type s-SWNTs. The error values increase with the increase of the tube diameter because $E_g \propto 1/d_{\mathrm{t}}$ and also because the formula for S_{CNT} [Eq. (2)] was derived by assuming s-SWNTs as nondegenerate semiconductors. Therefore, larger band gaps or smaller diameter s-SWNTs should be more accurately fitted by our S_{CNT} approximation.

[1] J. P. Heremans, M. S. Dresselhaus, L. E. Bell, and D. T. Morelli, Nat. Nanotechnol. **8**, 471–473 (2013).
[2] C. B. Vining, Nat. Mater. **8**, 83–85 (2009).
[3] A. Majumdar, Science **303**, 777–778 (2004).
[4] L. D. Hicks and M. S. Dresselhaus, Phys. Rev. B **47**, 16631–16634 (1993).
[5] L. D. Hicks, T. C. Harman, X. Sun, and M. S. Dresselhaus, Phys. Rev. B **53**, R10493–R10496 (1996).
[6] J. Hone, I. Ellwood, M. Muno, A. Mizel, Marvin L. Cohen, A. Zettl, Andrew G. Rinzler, and R. E. Smalley, Phys. Rev. Lett. **80**, 1042–1045 (1998).
[7] J. Hone, M. C. Llaguno, N. M. Nemes, A. T. Johnson, J. E. Fischer, D. A. Walters, M. J. Casavant, J. Schmidt, and R. E. Smalley, Appl. Phys. Lett. **77**, 666–668 (2000).
[8] K. Yanagi, S. Kanda, Y. Oshima, Y. Kitamura, H. Kawai, T. Yamamoto, T. Takenobu, Y. Nakai, and Y. Maniwa, Nano Lett. **14**, 6437–6442 (2014).
[9] H. E. Romero, G. U. Sumanasekera, G. D. Mahan, and P. C. Eklund, Phys. Rev. B **65**, 205410 (2002).
[10] H. L. Zhang, J. F. Li, B. P. Zhang, K. F. Yao, W. S. Liu, and H. Wang, Phys. Rev. B **75**, 205407 (2007).
[11] M. S. Dresselhaus, G. Chen, M. Y. Tang, R. G. Yang, H. Lee, D. Z. Wang, Z. F. Ren, J-P. Fleurial, and P. Gogna, Adv. Mater. **19**, 1043–1053 (2007).
[12] B. Poudel, Q. Hao, Y. Ma, Y. Lan, A. Minnich, B. Yu, X. Yan, D. Wang, A. Muto, D. Vashaee, X. Chen, J. Liu, M. S. Dresselhaus, G. Chen, and Ren Z., Science **320**, 634–638 (2008).
[13] R. Saito, G. Dresselhaus, and M. S. Dresselhaus, *Physical Properties of Carbon Nanotubes* (Imperial College Press, London, 1998).
[14] Y. Nakai, K. Honda, K. Yanagi, H. Kataura, T. Kato, T. Yamamoto, and Y Maniwa, Appl. Phys. Express **7**, 025103 (2014).
[15] H. Suzuura and T. Ando, Phys. Rev. B **65**, 235412 (2002).
[16] A. Javey, J. Guo, M. Paulsson, Q. Wang, D. Mann, M. Lundstrom, and H. Dai, Phys. Rev. Lett. **92**, 106804 (2004).
[17] J. Jiang, R. Saito, Ge. G. Samsonidze, S. G. Chou, A. Jorio, G. Dresselhaus, and M. S. Dresselhaus, Phys. Rev. B **72**, 235408 (2005).
[18] G. K. H. Madsen and D. J. Singh, Comput. Phys. Commun. **175**, 67–71 (2006).
[19] H. J. Goldsmid and J. W. Sharp, J. Electron. Mater. **28**, 869–872 (1999).
[20] H. Julian Goldsmid, *Introduction to Thermoelectricity* (Springer-Verlag, Berlin Heidelberg, 2010).
[21] Ge. G. Samsonidze, R. Saito, N. Kobayashi, A. Grüneis, J. Jiang, A. Jorio, S. G. Chou, G. Dresselhaus, and M. S. Dresselhaus, Appl. Phys. Lett. **85**, 5703–5705 (2004).
[22] V. N. Popov, New. J. Phys **6**, 17 (2004).
[23] R. B. Weisman and S. M. Bachilo, Nano Lett. **3**, 1235–1238 (2003).
[24] R. B. Capaz, C. D. Spataru, P. Tangney, M. L. Cohen, and S. G. Louie, Phys. Rev. Lett. **94**, 036801 (2005).
[25] A. Shakouri, Annu. Rev. Mater. Res. **41**, 399–431 (2011).
[26] A. I. Boukai, Y. Bunimovich, J. Tahir-Kheli, J. Yu, W. A. Goddard III, and J. R. Heath, Nature **451**, 168–171 (2008).
[27] J. P. Heremans, V. Jovovic, E. S. Toberer, A. Saramat, K. Kurosaki, A. Charoenphakdee, S. Yamanaka, and G. J. Snyder, Science **321**, 554–557 (2008).
[28] Y. Pei, X. Shi, A. LaLonde, H. Wang, L. Chen, and G. J. Snyder, Nature **473**, 66–69 (2011).
[29] R. Saito, G. Dresselhaus, and M. S. Dresselhaus, Phys. Rev. B **61**, 2981–2990 (2000).
[30] H. Kataura, Y. Kumazawa, Y. Maniwa, I. Umezu, S. Suzuki, Y. Ohtsuka, and Y. Achiba, Synthetic Met. **103**, 2555–2558 (1999).
[31] H. Liu, D. Nishide, T. Tanaka, and H. Kataura, Nat. Commun. **2**, 309 (2011).
[32] H. Liu, T. Tanaka, Y. Urabe, and H. Kataura, Nano Lett. **13**, 1996–2003 (2013).